Gate Direct Tunneling Current in Uniaxially Compressive Strained nMOSFETs: A Sensitive Measure of Electron Piezo Effective Mass

Wei-Han Lee, *Student Member, IEEE*, and Ming-Jer Chen, *Senior Member, IEEE*

***Abstract*—Currently, both the band-structure calculation and the mobility measurement are used to assess the electron piezo-effective-mass coefficients in strained nMOSFETs. In this paper, we present a new experimental method through a fitting of the strain-altered electron gate direct tunneling current. The core of this method lies in the sensitivity of the direct tunneling to the position of the subband level in the presence of the electron piezo-effective-mass coefficients. First, a correction-coefficient generating expression is systematically constructed to compensate for the error in the subband levels due to the use of a triangular potential approximation. Then, with the known deformation potential constants and uniaxially compressive stress in the channel as inputs, a strain quantum simulator is carried out. The resulting gate direct tunneling current is used to fit experimental data, thus leading to the values of the piezo-effective-mass coefficients associated with the twofold and fourfold valleys. The comparison of the extracted piezo-effective-mass coefficients to those published in the literature is made.**

***Index Terms*—Effective mass, mechanical stress, MOSFET, piezo, quantum confinement, tunneling, uniaxially compressive strain.**

I. Introduction

FOR SILICON n-type metal–oxide–semiconductor field-effect transistors (nMOSFETs) formed on (001) substrate, the quantum confinement effect [1] around the inversion layer makes the bulk conduction band split into two distinctive components: 1) a twofold (Δ_2) valley and 2) a fourfold (Δ_4) valley. The longitudinal effective mass (m_l) and transverse effective mass (m_t) associated with those subband valleys essentially remain intact [1]. The energetic difference between Δ_2 and Δ_4 levels can further be changed through the applied mechanical stress as in the state-of-the-art strain engineering. The stress-induced subband shift has thoroughly been theoretically studied [2] in terms of the deformation potential constants [3]–[5]. Recently, a sophisticated band-structure calculation [6]–[8] on (001) silicon surface has pointed out that only with the strain dependence of m_l and m_t taken into account can the strain-induced mobility change be elucidated. The significance of the strain-dependent electron effective masses in the (110) case has also been mentioned [9]. Thus, in addition to the deformation potential counterparts, the strain dependence of m_l and m_t or, equivalently, the electron piezo-effective-mass coefficient, π_m, should not be absent in the strain-altered conduction-band structure.

So far, the mobility measurement method has been constructed to experimentally determine the π_m of the inversion-layer electrons [10]. On the other hand, the effect of the mechanical stress on the electron gate tunneling current has experimentally been observed [11]–[17]. In the citations [11]–[17], however, the impact of the π_m on the electron gate tunneling current has not been noticed. According to the quantum confinement picture [1], a change in the electron quantization effective mass due to the stress produces a change in the subband level, which will, in turn, dramatically change the transmission probability. Thus, through the inverse modeling technique, the electron gate direct tunneling current in strained devices should, in principle, serve as a sensitive detector of π_m. However, few studies on this subject were done to date.

The aim of this paper is to assess the π_m through the fitting of the measured electron gate direct tunneling current change in uniaxially compressive strained nMOSFETs, which will be carried out in a triangular potential approximation due to its widespread use. To compensate for the subband level for the use of the triangular potential approximation and hence ensure the data fitting quality, a correction-coefficient generating expression will systematically be established. Then, a strain quantum simulator dedicated to the electron gate direct tunneling will be performed. To practically demonstrate the fitting process, we will make use of the literature data stemming from the externally applied [14] and process-induced [16] uniaxial compressive stress (001) nMOSFETs. The resulting π_m will be given, followed by the comparison with those obtained by the band-structure calculation [6]–[8] and the mobility measurement [10].

II. Correction Coefficient Generator

In the context of the triangular potential approximation as characterized by a surface field F_s, the solving of the Schrödinger equation in the quantum-confined direction normal

Manuscript received May 26, 2010; revised September 24, 2010; accepted September 25, 2010. Date of publication November 9, 2010; date of current version December 27, 2010. This work was supported by the National Science Council of Taiwan under Contract NSC 97-2221-E-009-155-MY3. The review of this paper was arranged by Editor A. M. Ionescu.

The authors are with the Department of Electronics Engineering and the Institute of Electronics, National Chiao Tung University, Hsinchu 300, Taiwan (e-mail: chenmj@faculty.nctu.edu.tw).

Color versions of one or more of the figures in this paper are available online at http://ieeexplore.ieee.org.

Digital Object Identifier 10.1109/TED.2010.2084578

to the SiO_2/Si surface yields Δ_2 subband level i in the absence of the stress [1]. We have

$$E_{\Delta 2,i} = \left(\frac{\hbar^2}{2m_{z,\Delta 2}}\right)^{\frac{1}{3}} \left(\frac{3}{2}\pi q F_s \left(i - \frac{1}{4}\right)\right)^{\frac{2}{3}} \quad (1)$$

where $m_{z,\Delta 2}$ is the Δ_2 quantization effective mass. Equation (1) can apply to fourfold case by replacing Δ_2 with Δ_4. To examine the validity of the triangular potential approximation, a self-consistent Poisson–Schrödinger equations solver, *Schred* [18], was used. The resulting conduction potential profile is shown in Fig. 1, along with the five lowest subband levels. In the figure, the drawback of the conventional triangular potential approximation is clear, particularly in the higher energy levels, where the corresponding electric field deviates from the surface field F_s. To address this issue, different methods have previously been proposed: 1) the variation approach dedicated to the correction of the lowest subband [1], [19] and 2) the effective field F_{eff}, instead of F_s, in (1) [14], [16], [20]–[23], i.e.,

$$F_{\text{eff}} = \frac{\eta Q_{\text{inv}} + Q_{\text{dep}}}{\varepsilon_{\text{si}}} \quad (2)$$

where Q_{inv} is the inversion-layer charge density, Q_{dep} is the bulk depletion charge density, and ε_{si} is the silicon permittivity. The correction coefficient η in (2) is constant with a spanned range from 0.5 to 1.0: $\eta = 0.75$ for Δ_2 and 1.0 for Δ_4 [14], [16], $\eta = 0.5$ for all subbands [20], and $\eta = 0.75$ for all subbands [21]–[23]. However, the previous improvements that led to (2) are not enough, because from the aspect of the direct tunneling, each of the subbands involved in the tunneling should have its own correction coefficient such as to ensure the proper direct tunneling calculation. Obviously, due to different electric fields encountered from level to level as revealed in Fig. 1, different correction coefficient values should correspond to different subbands. To take this into account, we suggest the individual correction coefficient $\eta_{\Delta 2,i}$ for Δ_2 level i, and the corresponding effective electric field can be written as

$$F_{\Delta 2,i} = \frac{\eta_{\Delta 2,i} Q_{\text{inv}} + Q_{\text{dep}}}{\varepsilon_{\text{si}}}. \quad (3)$$

The same procedure can apply to the Δ_4 case: $F_{\Delta 4,i}$ corresponds to $\eta_{\Delta 4,i}$. Again, to quantify the correction coefficient values, the solver *Schred* [18] was conducted in a metal–oxide–semiconductor (MOS) system on (001) silicon surface. The following key process parameters were included: 1) the substrate doping concentration, $N_{\text{sub}} = 10^{15}, 10^{16}, 10^{17}$, and 10^{18} cm^{-3}; 2) the gate oxide thickness, $t_{\text{ox}} = 1$, 3, and 6 nm; and 3) the different gate stacks in terms of a polysilicon and a metal electrode. By matching the subband levels produced by *Schred* with those from (1), with F_s replaced by $F_{\Delta 2,i}$ for the twofold valley and $F_{\Delta 4,i}$ for the fourfold valley, the values of the $\eta_{\Delta 2,i}$ and $\eta_{\Delta 4,i}$ result. A scatter plot between the correction coefficient values and the corresponding subband levels is given in Fig. 2, which is made with the surface field F_s as a parameter. Strikingly, the figure points to two relevant relationships. First, under fixed F_s, all data points fall on or around a straight line, indicating that the correction coefficient linearly depends on the subband level. Second, the straight

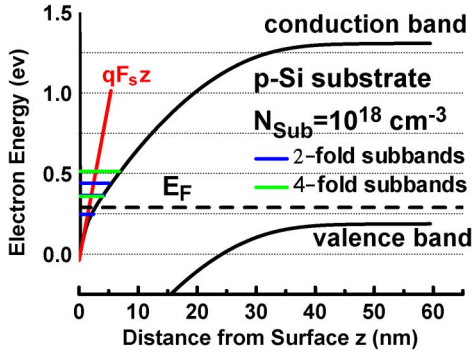

Fig. 1. Silicon energy-band diagram near the SiO_2/Si surface produced by the simulator *Schred* [18] (black solid lines), along with the five lowest subband levels (blue solid lines for Δ_2 and green solid lines for $\Delta 4$) and the Fermi level (dotted line), as well as the straight line (red line) for the triangular potential approximation under the same surface field F_s of 2 MV/cm as that of *Schred*.

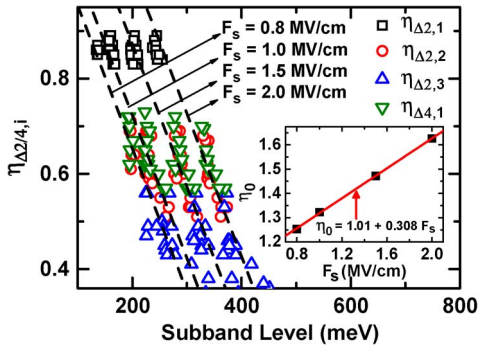

Fig. 2. Extracted correction coefficient versus the corresponding subband level, with the surface field as a parameter. The fitting lines are drawn. The intercept, η_o, of the extrapolated line at the zero-subband level is inserted and plotted versus the surface field. A fitting line is also shown in the inset.

line appears to shift with F_s. This specific behavior can be modeled by the intercept, designated as η_o, of the extrapolated line at the zero-subband level. In the inset of the figure, η_o is plotted against F_s, clearly showing another linear relationship, regardless of the N_{sub}, t_{ox}, or gate stack material. This result is expected from the aspect of the MOS electrostatics. The combination of these two linear relationships therefore leads to a subband-level correction-coefficient-generating expression suitable for both Δ_2 and Δ_4, i.e.,

$$\eta_{\Delta 2/4,i} = -0.003 E_{\Delta 2/4,i} + (1.01 + 0.308 F_s). \quad (4)$$

The units of $E_{\Delta 2/4,i}$ and F_s in (4) are given in millielectronvolts and megavolts per centimeter, respectively. Equation (4) can provide a transparent understanding of the effect of the subband level and surface field on the calculated correction coefficient. Interestingly, (4) is also self consistent, because for those of the subband levels close to the reference point (that is, the classical conduction band edge at the surface), the correction coefficients lie in the close proximity of unity, and hence, the effective electric field approaches the surface one. To testify to the validity of (4) in the subband level calculation, the results are compared with those from *Schred* [18], as given in Fig. 3 for two different gate stacks. Excellent agreements are evident, obtained without adjusting any parameters. Note that

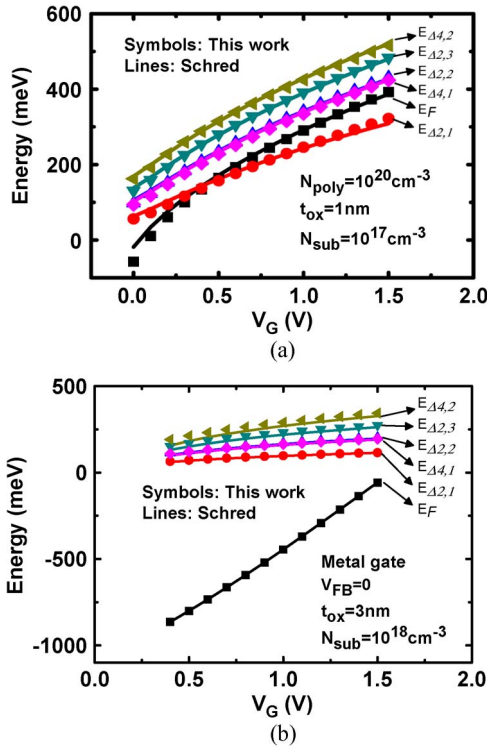

Fig. 3. Subband levels calculated by the triangular potential approximation based on the new η correction generator (solid dots) and by *Schred* (lines) for two cases: (a) n+ polysilicon doping $N_{poly} = 10^{20}$ cm^{-3}, $t_{ox} = 1$ nm, and $N_{sub} = 10^{17}$ cm^{-3} and (b) metal gate with zero flatband voltage, $t_{ox} = 3$ nm, and $N_{sub} = 10^{18}$ cm^{-3}.

the expression (4) is valid only for the (001) substrate. Further study is needed to examine the underlying physical origins and the applicability of the two linear relationships in Fig. 2 in case of different substrate orientations.

III. Strain Quantum Simulator

The correction coefficient generator (4) was incorporated into a strain quantum simulator in our previous works [24], [25]. The resulting subband level in the presence of the uniaxial channel stress σ in the $\langle 110 \rangle$ direction can be written with respect to the nonstress conduction-band edge at the Si/SiO$_2$ interface [3]–[5], [14] as follows:

$$E'_{\Delta 2,i} = E_{\Delta 2,i} + \left(\Xi_d + \frac{\Xi_u}{3}\right)(S_{11} + 2S_{12})\sigma + \left(\frac{\Xi_u}{3}\right)(S_{12} - S_{11})\sigma \quad (5)$$

$$E'_{\Delta 4,i} = E_{\Delta 4,i} + \left(\Xi_d + \frac{\Xi_u}{3}\right)(S_{11} + 2S_{12})\sigma - \left(\frac{\Xi_u}{6}\right)(S_{12} - S_{11})\sigma \quad (6)$$

where the elastic compliance constants $S_{11} = 7.68 \times 10^{-12}$ m^2/N and $S_{12} = -2.14 \times 10^{-12}$ m^2/N, and the hydrostatic and shear deformation potential constants $\Xi_d = 1.13$ eV and $\Xi_u = 9.16$ eV [26]. The effect of different deformation potential constants will later be described. The

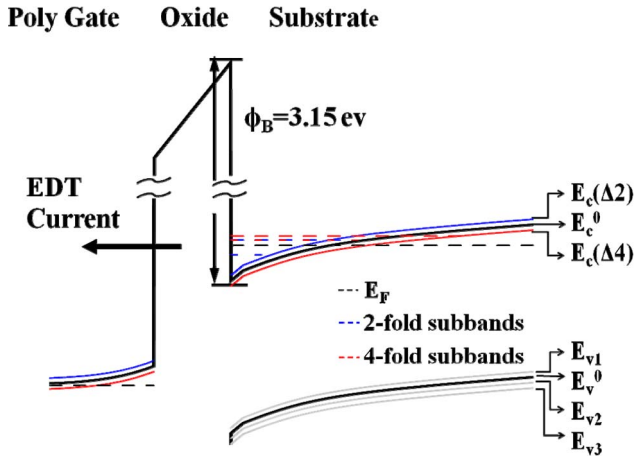

Fig. 4. Schematic energy-band diagram of the n+ polysilicon/SiO$_2$/p-Si MOS system under uniaxial compressive stress along $\langle 110 \rangle$ on the (001) substrate. The black solid lines represent the conduction and valence band edge without the stress. The blue and green solid lines represent the stress induced conduction band splits. The EDT current from the subband levels is also shown.

carrier repopulation under stress can accordingly be calculated [27] as follows:

$$N_{\Delta 2/4,i} = g_{\Delta 2/4}\left(\frac{m_{d,\Delta 2/4} k_B T}{\pi \hbar^2}\right) \times \ln\left(1 + \exp\left(\frac{E_F - E'_{\Delta 2/4,i}}{k_B T}\right)\right) \quad (7)$$

where $g_{\Delta 2/4}$ is the Δ_2 (Δ_4) valley degeneracy, $m_{d,\Delta 2/4}$ is the 2-D density-of-states (DOS) effective mass of the Δ_2 (Δ_4) valley, E_F is the electron Fermi level, k_B is the Boltzmann constant, and T is the absolute temperature. Finally, the electron gate direct tunneling current density can be computed from the following expression, which can be deduced from the unstrained case [19], [24]:

$$J_e = \sum_i q f_{\Delta 2,i} N_{\Delta 2,i} P_t\left(E'_{\Delta 2,i}\right) + \sum_i q f_{\Delta 4,i} N_{\Delta 4,i} P_t\left(E'_{\Delta 4,i}\right) \quad (8)$$

where f represents the electron impact frequency on the Si/SiO$_2$ interface and is equal to $(qF_{\Delta 2/4,i}/2)(2m_{z,\Delta 2/4} E_{\Delta 2/4,i})^{-1/2}$, and $P_t(E'_{\Delta 2/4,i})$ is the electron transmission probability across the SiO$_2$ film. In Fig. 4, the energy band diagram of the MOS system under study is schematically shown, where the electron direct tunneling (EDT) process from the subband level is highlighted. Throughout this paper, only five lowest subbands (three subbands of Δ_2 and two subbands of Δ_4) will be adopted to calculate the gate current. The accuracy of the calculated gate current will later be addressed.

Here, the electron effective mass in the oxide for the parabolic-type dispersion relationship was used with $m_{ox} = 0.50\ m_o$, which is equivalent to $m_{ox} = 0.61\ m_o$ for the tunneling electrons in the oxide using the Franz-type dispersion relationship [28]. The SiO$_2$/Si interface barrier height in the absence of stress is 3.15 eV. Given the situations that the deformation potential constants are known and the uniaxial

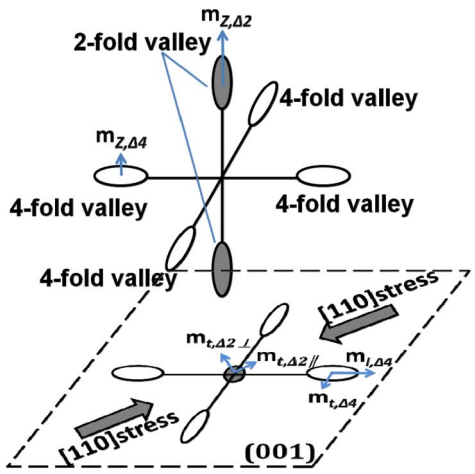

Fig. 5. Schematic silicon conduction-band structure in terms of six constant-energy surfaces in the Brillouin zone. The electron effective masses in the presence of a uniaxial compressive stress are also labeled.

TABLE I
NOMINAL VALUES OF THE UNSTRAINED ELECTRON EFFECTIVE MASSES USED IN THIS PAPER AND THE REFERENCES [6]–[8], [10]

	[6]	[7]	[8]	[10]	This work
$m_{z,\Delta 2}$		0.918	0.916		0.916
$m_{t,\Delta 2\parallel}$	0.2	0.196	0.194		0.19
$m_{t,\Delta 2\perp}$	0.2	0.196	0.194		0.19
$m_{d,\Delta 2}$	0.2	0.196	0.194		0.19
$m_{z,\Delta 4}$					0.19
$m_{l,\Delta 4}$	0.89				0. 916
$m_{t,\Delta 4}$	0.2				0.19
$m_{d,\Delta 4}$	0.42				0.417

Units: m_0/GPa.
Oblique line: Not available.

channel stress can be determined by other means, we have the following four variables in using (8) to quantify the gate direct tunneling current: 1) the twofold quantization effective mass $m_{z,\Delta 2}$; 2) the twofold 2-D DOS effective mass $m_{d,\Delta 2}$; 3) the fourfold quantization effective mass $m_{z,\Delta 4}$; and 4) the fourfold 2-D DOS effective mass $m_{d,\Delta 4}$. The DOS effective mass can relate to the aforementioned m_l and m_t of the valley: $m_{d,\Delta 2} = (m_{t,\Delta 2\parallel} m_{t,\Delta 2\perp})^{1/2}$ and $m_{d,\Delta 4} = (m_{l,\Delta 4} m_{t,\Delta 4})^{1/2}$. Here, $m_{t,\Delta 2\parallel}$ and $m_{t,\Delta 2\perp}$ are the in-plane transverse effective mass of Δ_2 in the direction parallel and perpendicular to the stress direction, respectively, and $m_{l,\Delta 4}$ and $m_{t,\Delta 4}$ are the in-plane longitudinal and transverse effective mass of Δ_4, respectively. All the effective masses involved in this paper are depicted in Fig. 5 in terms of the conduction-band structure in the Brillouin zone. The corresponding nominal values (i.e., in the absence of the stress) are listed in Table I.

IV. DATA FITTING

The measured electron gate direct tunneling current change due to the externally applied uniaxial compressive stress as cited in [14] is plotted in Fig. 6 for three different gate voltages. In addition, Fig. 6 plots the calculated results using the nominal effective mass values only, which do not appear to agree with the data in a wide range of stress and gate voltage. Although we tried other different nominal values for the effective masses in silicon, the deformation potential constants, the effective mass in the oxide, the doping concentration, and the gate oxide thickness, a poor fitting such as in Fig. 6 still remained.

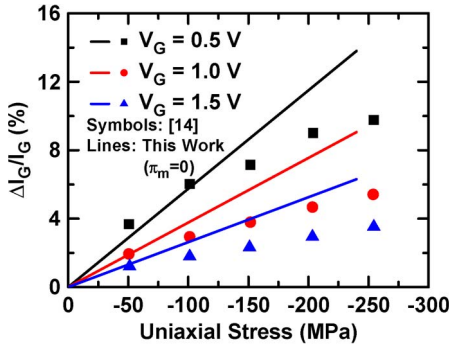

Fig. 6. Comparisons of the measured (symbols) gate current change due to the external uniaxially compressive stress [14] with the calculated (lines) ones obtained using the nominal values in Table I for the electron effective masses. The process parameters used are $N_{sub} = 10^{17}$ cm^{-3}, tox = 1.3 nm, and $N_{ploy} = 10^{20}$ cm^{-3}. Poor fitting is encountered if the piezo-effective-mass coefficients are not included.

Obviously, for a general effective mass m, the piezo-effective-mass coefficient π_m must be added as follows:

$$m_z(\sigma) = m_z(0) + \pi_{m,z}\sigma \tag{9}$$

$$m_d(\sigma) = m_d(0) + \pi_{m,d}\sigma. \tag{10}$$

Here, we impose a small stress to make possible a linear approximation and thus ensure the validity of (9) and (10). To assess the underlying π_m ($\pi_{m,z\Delta 2}$, $\pi_{m,d\Delta 2}$, $\pi_{m,z\Delta 4}$, and $\pi_{m,d\Delta 4}$), a sensitivity analysis was performed during the data fitting. First, one of four π_m factors was alternately selected in applying (9) or (10), with the remaining three factors kept at zero. Strikingly, we found that the $\pi_{m,z\Delta 4}$ is the primary factor, because it can have the strongest effect on the calculated gate current change, as illustrated in Fig. 7 for $\pi_{m,z\Delta 4}$ of 0.03, 0.05, and 0.07 m_o/GPa. It is shown in the figure that the fitting can be somewhat improved by simply increasing $\pi_{m,z\Delta 4}$. Next, we also found that the $\pi_{m,d\Delta 2}$ can serve as the secondary factor in refining the calculated gate current change. This condition means that both $\pi_{m,z\Delta 4}$ and $\pi_{m,d\Delta 2}$ are enough in producing the reasonable fitting. Thus, in the subsequent work, we set $\pi_{m,z\Delta 2}$ and $\pi_{m,d\Delta 4}$ to zero. The following set of the $\pi_{m,z\Delta 4}$ and $\pi_{m,d\Delta 2}$ values was hence extracted from the best fitting, as displayed in Fig. 7: 1) $\pi_{m,z\Delta 4} = 0.03$ m_o/GPa, and $\pi_{m,d\Delta 2} = -0.03$ m_o/GPa; 2) $\pi_{m,z\Delta 4} = 0.05$ m_o/GPa, and $\pi_{m,d\Delta 2} = -0.02$ m_o/GPa; and 3) $\pi_{m,z\Delta 4} = 0.07$ m_o/GPa, and $\pi_{m,d\Delta 2} = -0.017$ m_o/GPa. Obviously, the increasing $\pi_{m,z\Delta 4}$ is accompanied with the less negative $\pi_{m,d\Delta 2}$. The piezo-effective-mass coefficient values obtained in the data fitting are listed in Table II.

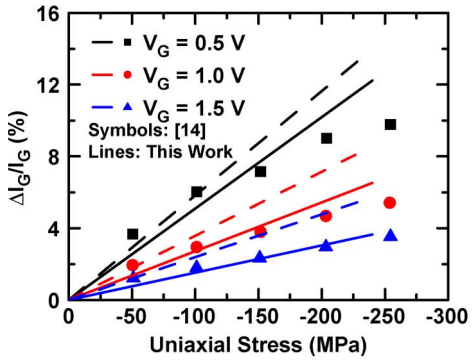

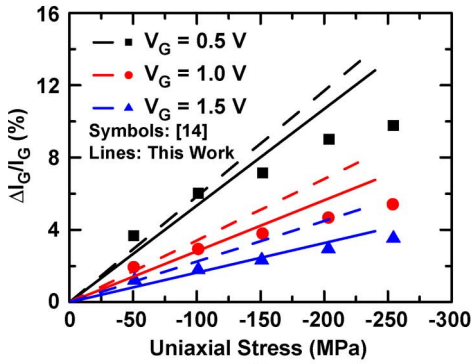

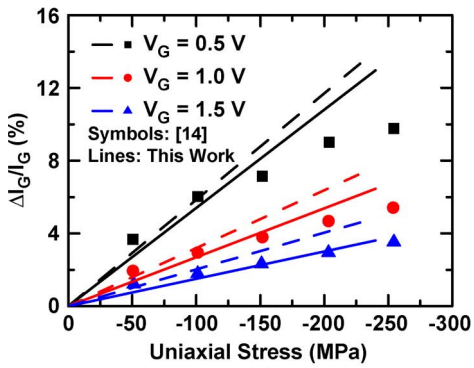

Fig. 7. Comparison of the data (symbols) [14] with the calculated results (lines) for (a) $\pi_{m,z\Delta 4} = 0.03$ m_0/GPa (dashed lines); and $\pi_{m,z\Delta 4} = 0.03$ m_0/GPa and $\pi_{m,d\Delta 2} = -0.03$ m_0/GPa (solid lines); (b) $\pi_{m,z\Delta 4} = 0.05$ m_0/GPa (dashed lines); and $\pi_{m,z\Delta 4} = 0.05$ m_0/GPa and $\pi_{m,d\Delta 2} = -0.02$ m_0/GPa (solid lines); and (c) $\pi_{m,z\Delta 4} = 0.07$ m_0/GPa (dashed lines); and $\pi_{m,z\Delta 4} = 0.07$ m_0/GPa and $\pi_{m,d\Delta 2} = -0.017$ m_0/GPa (solid lines). $\pi_{m,z\Delta 2}$ and $\pi_{m,d\Delta 4}$ both are zero.

TABLE II
COMPARISON OF THE ELECTRON PIEZO-EFFECTIVE-MASS COEFFICIENTS FROM THE BAND-STRUCTURE CALCULATION AND MOBILITY MEASUREMENT [6]–[8], [10] WITH THOSE OBTAINED IN THIS PAPER. THE MECHANICAL STRESS IS APPLIED ALONG THE ⟨110⟩ DIRECTION ON THE (001) SILICON SURFACE

	[6] [compressive]	[6] [tensile]	[7] [tensile]	[8] [tensile]	[10] [tensile]	This Work [compressive]
$\pi_{m,t\Delta 2\,//}$	-0.014#	-0.012#	-0.016	-0.012#	-0.048	
$\pi_{m,t\Delta 2\perp}$	0.013#	0.014#	0.029	0.013#	0.029	
$\pi_{m,z\Delta 2}$			0.0071#	0.002#		~ 0
$\pi_{m,d\Delta 2}$	0.0005	0.001	0.0065	0.0005	-0.0095	-0.03 ~ -0.017
$\pi_{m,l\Delta 4}$	0.0026	0.0024				
$\pi_{m,t\Delta 4}$	0.001	0.001				
$\pi_{m,z\Delta 4}$						0.03 ~ 0.07
$\pi_{m,d\Delta 4}$	0.0017	0.0016				~ 0

#: Linear approximation over a range of <110> uniaxial stress σ on (001) substrate from 0 to 300 or -300 MPa.
Units: m_0/GPa.

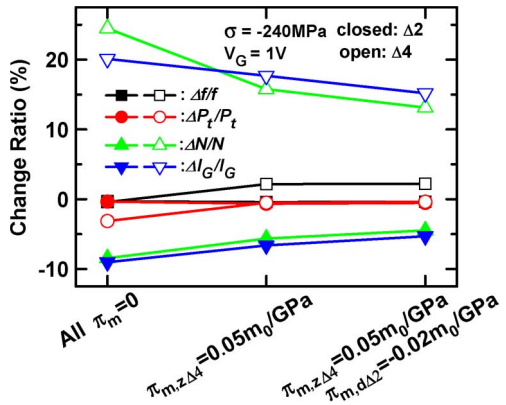

Fig. 8. Calculated gate current change ratio and its decoupling into different components: the impact frequency $f_{\Delta 2/4}$, the transmission probability $P_{t,\Delta 2/4}$, and the electron density $N_{\Delta 2/4}$. The repopulation of the valley is the main factor responsible for the gate current change.

Here, we give plausible explanations for the assessed $\pi_{m,z\Delta 4}$ and $\pi_{m,d\Delta 2}$ and, particularly, the difference in the polarity between the two. First, a positively increased $\pi_{m,z\Delta 4}$ will decrease the Δ_4 quantization effective mass [see (9)] under uniaxial compressive stress, which will, in turn, increase the Δ_4 level. As a result, due to the repopulation of the valley, more electrons are transferred down to the Δ_2 subband, and hence, the direct tunneling is reduced. Second, a less negative $\pi_{m,d\Delta 2}$ will increase the *effective* DOS in Δ_2 [see (10)] under uniaxial compressive stress. Thus, the increased population in Δ_2 dictates that the gate direct tunneling is reduced. To corroborate this condition, additional work was done by decoupling the gate current change into different components according to (8). The results are depicted in Fig. 8. One can see in Fig. 8 that the repopulation is the main factor that affects the calculated gate current change. Again, here, we want to stress that, even with only the *three* lowest subbands (two subbands of Δ_2 and 1 subband of Δ_4) used in the gate current calculation, little change in the listed π_m in Table II can occur. In this sense, the total number of the six lowest subbands remains valid.

V. COMPARISON AND DISCUSSION

The published formalisms and/or graphical data in the citations [6]–[8], [10] can furnish the quantified π_m of the longitudinal effective mass m_l and the transverse effective mass m_t for twofold and fourfold valleys, except for the fourfold quantization one. To determine the corresponding DOS π_m,

we derived the following analytical expressions from the linear approximation in (9) and (10):

$$\pi_{md,\Delta 2} = \frac{1}{2}\left(\frac{\pi_{mt,\Delta 2//}}{m_{t,\Delta 2//}} + \frac{\pi_{mt,\Delta 2\perp}}{m_{t,\Delta 2\perp}}\right)\sqrt{m_{t,\Delta 2//} m_{t,\Delta 2\perp}} \tag{11}$$

$$\pi_{md,\Delta 4} = \frac{1}{2}\left(\frac{\pi_{ml,\Delta 4}}{m_{l,\Delta 4}} + \frac{\pi_{mt,\Delta 4}}{m_{t,\Delta 4}}\right)\sqrt{m_{l,\Delta 4} m_{t,\Delta 4}}. \tag{12}$$

The results are added to Table II. Although the strain dependence of the fourfold quantization effective mass was not provided in the studies [6]–[8], [10], and hence, it is impossible to directly examine the validity of the extracted $\pi_{m,z\Delta 4}$ in this paper, some comparisons can still be made through Table II. First, the published values of $\pi_{m,z\Delta 2}$ and $\pi_{m,d\Delta 4}$ [6]–[8], [10] are very small in magnitude, which support the hypothesis of approximately zero $\pi_{m,z\Delta 2}$ and $\pi_{m,d\Delta 4}$ in the aforementioned data fitting. Indeed, we found that little change in the assessed $\pi_{m,z\Delta 4}$ and $\pi_{m,d\Delta 2}$ can be observed if the literature values of $\pi_{m,z\Delta 2}$ and $\pi_{m,d\Delta 4}$ [6]–[8], [10] are used instead. Second, the assessed $\pi_{m,d\Delta 2}$ is negative, quite close to that (-0.0095 m_o/GPa) obtained from the mobility measurement [10]. Finally, Table II provides the maximum π_m in magnitude available to date, i.e., 0.048 m_o/GPa [10]. In comparison, the assessed $\pi_{m,z\Delta 4}$ (ranging from 0.03 to 0.07 m_o/GPa) in this paper seems to quantitatively be reasonable. Note that, according to (11), a negative $\pi_{m,d\Delta 2}$ means that at least one of $\pi_{m,t\Delta 2\|}$ and $\pi_{m,t\Delta 2\perp}$ is negative and its magnitude is larger than another having the positive value.

To strengthen the applicability of the assessed π_m, we further cite the previous work [16] in terms of the measured electron gate direct tunneling current change due to the process-induced uniaxial compressive channel stress, as shown in Fig. 9. In addition, Fig. 9(a) depicts the calculated results using the assessed π_m, exhibiting a large deviation from the data points. This condition is expected, because in the manufacturing process with the built-in stressors, the devices may encounter additional effects such as the stress-induced dopant redistribution [29] and the stress-induced thermal oxidation change [25], which are apparently not present in case of the external stress [14]. Here, we attribute this significant difference to the decrease in the gate oxide thickness of the device undergoing the process-induced uniaxial compressive stress. The physical interpretations are that the oxide growth rate will be retarded under the influence of the compressive stress in the manufacturing process. In this sense, one can define a piezo-oxide-thickness coefficient $\pi_{\rm tox}$ as follows:

$$t_{\rm ox}(\sigma) = t_{\rm ox}(0) + \pi_{\rm tox}\sigma. \tag{13}$$

The data were again fitted, leading to $\pi_{\rm tox}$ of 0.012 nm/GPa. The quality of the fitting, as demonstrated in Fig. 9(b), is fairly good. In addition, the extracted $\pi_{\rm tox}$ is reasonable compared to that ($\sim$0.02 nm/GPa) of the p-channel counterparts on the same test wafer [25].

Therefore, it is claimed that, due to the corroborating evidence in terms of the literature π_m values [6]–[8], [10] and the oxide thickness retardation [25], the electron gate direct tunneling current fitting as the sensitive detector of π_m in uniaxially compressive strained device is judged. Finally, we want to stress that the fit to process-induced data [16] works well [see Fig. 9(b)], whereas there is quite a large discrepancy in the fit to external stress data [14] (Fig. 7), particularly at lower gate voltage. To address this issue, we suggest that the stress distribution in the quoted device under the external stress [14] is nonuniform. This argument can be drawn from the calculated results in Fig. 7, which clearly point out that the stress effect of the gate current change is enhanced with decreasing gate voltage. Oppositely, this effect becomes weak for larger gate voltage. Thus, the gate current change due to a local stress variation may be amplified if the gate voltage applied is as low as 0.5 V. Relatively, for higher gate voltage at 1 V, the local stress variation accordingly produces little change in gate current. Fairly good agreement over the stress in Fig. 7 for gate voltage of 1 V supports this approach. In a sense, the gate voltage factor in the proposed gate current method can be helpful in clarifying the responsible mechanisms.

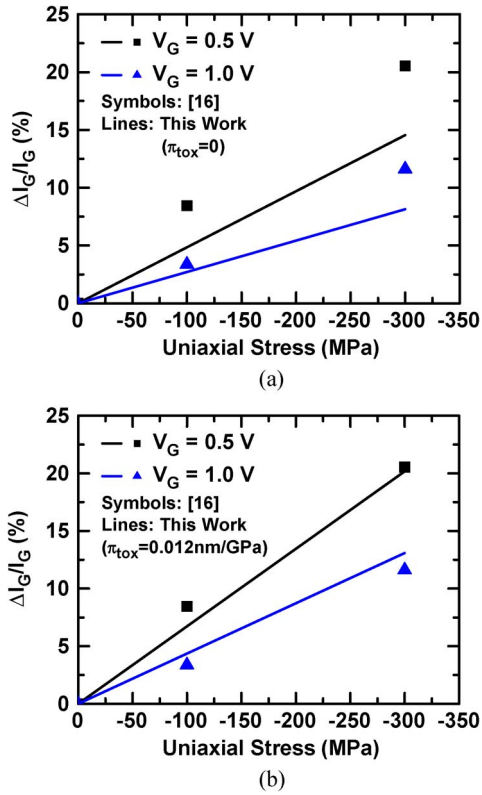

Fig. 9. Comparisons of the measured (symbols) [16] and calculated (lines) gate current change due to the process-induced compressive stress in the $\langle 110\rangle$ direction. The calculated results come from (a) $\pi_{\rm tox} = 0$ and (b) $\pi_{\rm tox} = 0.012$ nm/GPa. The piezo-effective-mass coefficients used correspond to Fig. 7(c): $\pi_{m,z\Delta 4} = 0.07$ m_0/GPa, $\pi_{m,d\Delta 2} = -0.017$ m_0/GPa, $\pi_{m,z\Delta 2} = 0$, and $\pi_{m,d\Delta 4} = 0$.

VI. Conclusion

A new correction-coefficient generator has systematically been created to compensate for the subband levels for the use of the triangular potential approximation. Then, with the known deformation potential constants and uniaxial compressive channel stress as inputs, the strain quantum simulation

dedicated to the gate direct tunneling current has rigorously been performed. Reasonable reproduction of the measured gate direct tunneling current has been achieved, leading to the underlying electron piezo-effective-mass coefficients. The confirmative evidence has been presented in terms of the published piezo-effective-mass coefficient and oxide thickness retardation values. The ability of the electron gate direct tunneling current in uniaxially compressive strained device as a sensitive detector of the electron piezo-effective-mass has been verified.

REFERENCES

[1] F. Stern, "Self-consistent results for n-type Si inversion layers," *Phys. Rev. B, Condens. Matter*, vol. 5, no. 12, pp. 4891–4899, Jun. 1972.

[2] M. V. Fischetti and S. E. Laux, "Band structure, deformation potentials, and carrier mobility in strained Si, Ge, and SiGe alloys," *J. Appl. Phys.*, vol. 80, no. 4, pp. 2234–2252, Aug. 1996.

[3] C. Herring and E. Vogt, "Transport and deformation-potential theory for many-valley semiconductors with anisotropic scattering," *Phys. Rev.*, vol. 101, no. 3, pp. 944–961, Feb. 1956.

[4] I. Balslev, "Influence of uniaxial stress on the indirect absorption edge in silicon and germanium," *Phys. Rev.*, vol. 143, no. 2, pp. 636–647, Mar. 1966.

[5] C. G. Van de Walle and R. M. Martin, "Theoretical calculations of heterojunction discontinuities in the Si/Ge system," *Phys. Rev. B: Condens. Matter*, vol. 34, no. 8, pp. 5621–5634, Oct. 1986.

[6] K. Uchida, T. Krishnamohan, K. C. Saraswat, and Y. Nishi, "Physical mechanisms of electron mobility enhancement in uniaxial stressed MOSFETs and impact of uniaxial stress engineering in ballistic regime," in *IEDM Tech. Dig.*, 2005, pp. 129–132.

[7] S. Dhar, E. Ungersböeck, H. Kosina, T. Grasser, and S. Selberherr, "Electron mobility model for ⟨110⟩ stressed silicon including strain-dependent mass," *IEEE Trans. Nanotechnol.*, vol. 6, no. 1, pp. 97–100, Jan. 2007.

[8] E. Ungersboeck, S. Dhar, G. Karlowatz, V. Sverdlov, H. Kosina, and S. Selberherr, "The effect of general strain on the band structure and electron mobility of silicon," *IEEE Trans. Electron Devices*, vol. 54, no. 9, pp. 2183–2190, Sep. 2007.

[9] K. Uchida, A. Kinoshita, and M. Saitoh, "Carrier transport in (110) nMOSFETs: Subband structure, nonparabolicity, mobility characteristics, and uniaxial stress engineering," in *IEDM Tech. Dig.*, 2006, pp. 1019–1021.

[10] F. Rochette, M. Cassé, M. Mouis, G. Reimbold, D. Blachier, C. Leroux, B. Guillaumot, and F. Boulanger, "Experimental evidence and extraction of the electron mass variation in [110] uniaxially strained MOSFETs," *Solid State Electron.*, vol. 51, no. 11/12, pp. 1458–1465, Nov./Dec. 2007.

[11] S. Takagi, T. Mizuno, T. Tezuka, N. Sugiyama, T. Numata, K. Usuda, Y. Moriyama, S. Nakaharai, J. Koga, A. Tanabe, N. Hirashita, and T. Maeda, "Channel structure design, fabrication and carrier transport properties of strained-Si/SiGe-on-insulator (strained-SOI) MOSFETs," in *IEDM Tech. Dig.*, 2003, pp. 57–60.

[12] W. Zhao, A. Seabaugh, V. Adams, D. Jovanovic, and B. Winstead, "Opposing dependence of the electron and hole gate currents in SOI MOSFETs under uniaxial strain," *IEEE Electron Device Lett.*, vol. 26, no. 6, pp. 410–412, Jun. 2005.

[13] S. E. Thompson, G. Sun, Y. S. Choi, and T. Nishida, "Uniaxial-process-induced strained-Si: Extending the CMOS roadmap," *IEEE Trans. Electron Devices*, vol. 53, no. 5, pp. 1010–1020, May 2006.

[14] J. S. Lim, X. Yang, T. Nishida, and S. E. Thompson, "Measurement of conduction band deformation potential constants using gate direct tunneling current in n-type metal–oxide–semiconductor field-effect transistors under mechanical stress," *Appl. Phys. Lett.*, vol. 89, no. 7, pp. 073 509-1–073 509-3, Aug. 2006.

[15] T. Hoshii, S. Sugahara, and S. Takagi, "Effect of tensile strain on gate current of strained-Si n-channel metal–oxide–semiconductor field-effect transistors," *Jpn. J. Appl. Phys.*, vol. 46, no. 4B, pp. 2122–2126, Apr. 2007.

[16] C. Y. Hsieh and M. J. Chen, "Measurement of channel stress using gate direct tunneling current in uniaxially stressed nMOSFETs," *IEEE Electron Device Lett.*, vol. 28, no. 9, pp. 818–820, Sep. 2007.

[17] M. Saitoh, A. Kaneko, K. Okano, T. Kinoshita, S. Inaba, Y. Toyoshima, and K. Uchida, "Three-dimensional stress engineering in FinFETs for mobility/on-current enhancement and gate current reduction," in *VLSI Symp. Tech. Dig.*, Jun. 2008, pp. 18–19.

[18] Schred. [Online]. Available: http://nanohub.org/resources/schred

[19] N. Yang, W. K. Henson, J. R. Hauser, and J. J. Wortman, "Modeling study of ultrathin gate oxides using direct tunneling current and capacitance–voltage measurements in MOS devices," *IEEE Trans. Electron Devices*, vol. 46, no. 7, pp. 1464–1471, Jul. 1999.

[20] C. K. Park, C. Y. Lee, B. J. Moon, Y. H. Byun, and M. Shur, "A unified current–voltage model for long-channel nMOSFETs," *IEEE Trans. Electron Devices*, vol. 38, no. 2, pp. 399–406, Feb. 1991.

[21] Y. Ma, L. Liu, Z. Yu, and Z. Li, "Validity and applicability of triangular potential well approximation in modeling of MOS structure inversion and accumulation layer," *IEEE Trans. Electron Devices*, vol. 47, no. 9, pp. 1764–1767, Sep. 2000.

[22] Y. T. Hou, M. F. Li, Y. Jin, and W. H. Lai, "Direct tunneling hole currents through ultrathin gate oxides in metal–oxide–semiconductor devices," *J. Appl. Phys.*, vol. 91, no. 1, pp. 258–264, Jan. 2002.

[23] H. Abebe, E. Cumberbatch, H. Morris, and V. Tyree, "Compact models of the quantized subband energy levels for MOSFET device application," in *Proc. IEEE UGIM*, 2008, pp. 58–60.

[24] K. N. Yang, H. T. Huang, M. C. Chang, C. M. Chu, Y. S. Chen, M. J. Chen, Y. M. Lin, M. C. Yu, S. M. Jang, D. C. H. Yu, and M. S. Liang, "A physical model for hole direct tunneling current in p^+ poly-gate pMOSFETs with ultrathin gate oxides," *IEEE Trans. Electron Devices*, vol. 47, no. 11, pp. 2161–2166, Nov. 2000.

[25] C. Y. Hsu, C. C. Lee, Y. T. Lin, C. Y. Hsieh, and M. J. Chen, "Enhanced hole gate direct tunneling current in process-induced uniaxial compressive stress p-MOSFETs," *IEEE Trans. Electron Devices*, vol. 56, no. 8, pp. 1667–1673, Aug. 2009.

[26] J. S. Lim, S. E. Thompson, and J. G. Fossum, "Comparison of threshold-voltage shifts for uniaxial and biaxial tensile-stressed n-MOSFETs," *IEEE Electron Device Lett.*, vol. 25, no. 11, pp. 731–733, Nov. 2004.

[27] F. Stern and W. E. Howard, "Properties of semiconductor surface inversion layers in the electric quantum limit," *Phys. Rev.*, vol. 163, no. 3, pp. 816–835, Oct. 1967.

[28] Z. A. Weinberg, "On tunneling in metal–oxide–silicon structures," *J. Appl. Phys.*, vol. 53, no. 7, pp. 5052–5056, Jul. 1982.

[29] Y. M. Sheu, S. J. Yang, C. C. Wang, C. S. Chang, L. P. Huang, T. Y. Huang, M. J. Chen, and C. H. Diaz, "Modeling mechanical stress effect on dopant diffusion in scaled MOSFETs," *IEEE Trans. Electron Devices*, vol. 52, no. 1, pp. 30–38, Jan. 2005.

Wei-Han Lee (S'09) received the B.S. degree in electrophysics in 2005 from the National Chiao Tung University, Hsinchu, Taiwan, where he is currently working toward the Ph.D. degree in electronics engineering in the Department of Electronics Engineering and the Institute of Electronics.

His research interests include the characterization and modeling of strained-Si MOSFETs and the mismatch in nanoscale devices.

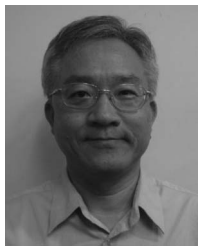

Ming-Jer Chen (S'78–M'79–SM'98) received the B.S. degree in electrical engineering (with highest honors) from the National Cheng-Kung University, Tainan, Taiwan, in 1977, and the M.S. and Ph.D. degrees in electronics engineering from the National Chiao Tung University (NCTU), Hsinchu, Taiwan, in 1979 and 1985, respectively.

Since 1985, he has been with the Department of Electronics Engineering and the Institute of Electronics, NCTU. He has become a Full Professor since 1993. From 1987 to 1992, he was a Consultant for the Taiwan Semiconductor Manufacturing Company, where he led a team from the NCTU and the Electronics Research and Service Organization/Industrial Technology Research Institute to build up a series of process windows and design rules. From 2000 to 2001, he was a Visiting Professor with the Department of Electrical Engineering and the Center for Integrated Systems, Stanford University, Stanford, CA. He is the holder of eight U.S. patents and six Taiwanese patents in high-precision analog capacitors, 1-T memory cell, dynamic threshold MOS, electrostatic discharge protection, and flash memory. He has graduated 15 Ph.D. students and more than 100 M.S. students. His current research interests include semiconductor device physics and nanoelectronics.

Dr. Chen is a member of the Phi Tau Phi.